

Supplementary Online Material to The Doring River Archaeology Project: Approaching the Evolution of Human Land Use Patterns in the Western Cape, South Africa

MATTHEW SHAW

Centre for Archaeological Science, School of Earth, Atmospheric and Life Sciences, University of Wollongong, Wollongong NSW 2522, AUSTRALIA; ms152@uowmail.edu.au

CHRISTOPHER J.H. AMES

Centre for Archaeological Science, School of Earth, Atmospheric and Life Sciences, University of Wollongong, Wollongong NSW 2522, AUSTRALIA; comes@uow.edu.au

NATASHA PHILLIPS

Centre for Archaeological Science, School of Earth, Atmospheric and Life Sciences, University of Wollongong, Wollongong NSW 2522, AUSTRALIA; np989@uowmail.edu.au

SHERRIE CHAMBERS

Centre for Archaeological Science, School of Earth, Atmospheric and Life Sciences, University of Wollongong, Wollongong NSW 2522, AUSTRALIA; sjrc913@uowmail.edu.au

ANTHONY DOSSETO

Centre for Archaeological Science, School of Earth, Atmospheric and Life Sciences, University of Wollongong, Wollongong NSW 2522, AUSTRALIA; tonyd@uow.edu.au

MATTHEW DOUGLAS

College of Agricultural Science and Natural Resources, University of Nebraska-Lincoln, Lincoln, NE 68583, USA; mdouglass3@unl.edu

RON GOBLE

Luminescence Geochronology Laboratory, 1400 R St., University of Nebraska-Lincoln, Lincoln, NE 68588, USA; rgoble2@unl.edu

ZENOBIA JACOBS

Centre for Archaeological Science, School of Earth, Atmospheric and Life Sciences; and, Australian Research Council Centre of Excellence for Australian Biodiversity and Heritage, University of Wollongong, Wollongong NSW 2522, AUSTRALIA; zenobia@uow.edu.au

BRIAN JONES

Centre for Archaeological Science, School of Earth, Atmospheric and Life Sciences, University of Wollongong, Wollongong NSW 2522, AUSTRALIA; briangj@uow.edu.au

SAM C.-H. LIN

Centre for Archaeological Science, School of Earth, Atmospheric and Life Sciences; and, Australian Research Council Centre of Excellence for Australian Biodiversity and Heritage, University of Wollongong, Wollongong NSW 2522, AUSTRALIA; samlin@uow.edu.au

MARIKA A. LOW

Centre for Archaeological Science, School of Earth, Atmospheric and Life Sciences, University of Wollongong, Wollongong NSW 2522, AUSTRALIA; marika.a.low@gmail.com

JESSICA-LOUISE MCNEIL

Department of Anthropology, Harvard University, Cambridge, MA 02138, USA; jlmcneil@g.harvard.edu

SHEZANI NASOORDEEN

Centre for Archaeological Science, School of Earth, Atmospheric and Life Sciences, University of Wollongong, Wollongong NSW 2522, AUSTRALIA; shezani@gmail.com

COREY A. O'DRISCOLL

Centre for Archaeological Science, School of Earth, Atmospheric and Life Sciences, University of Wollongong, Wollongong NSW 2522, AUSTRALIA; corey.odriscoll@outlook.com

ROSARIA B. SAKTURA

Centre for Archaeological Science, School of Earth, Atmospheric and Life Sciences, University of Wollongong, Wollongong NSW 2522, AUSTRALIA; rk693@uowmail.edu.au

T. ALEXANDRA SUMNER

Department of Anthropology, DePaul University, Chicago, IL 60614, USA; asummer2@depaul.edu

SARA WATSON

Department of Anthropology, University of California-Davis, Davis, CA 95616, USA; sewatson@ucdavis.edu

MANUAL WILL

Department of Early Prehistory and Quaternary Ecology, University of Tübingen, Schloss Hohentübingen, 72070 Tübingen, GERMANY; manuel.will@uni-tuebingen.de

ALEX MACKAY

Department of Archaeology, University of Cape Town, Rondebosch 8801, SOUTH AFRICA; amackay@uow.edu.au

submitted: 27 August 2019; accepted 6 October 2019

SUPPLEMENTARY ONLINE MATERIAL

SOM TABLE 1. ALL ARTIFACT ATTRIBUTES RECORDED DURING PHASE I.

Attribute	States	Applied to
Lithic Class	core, retouched flake, non-flaked	all
Implement Type	backed, bead, burin, core-on-flake, denticulate, grindstone, hammerstone, handaxe, notch, notch-complex, other, other-bifacial, <i>pièce esquille</i> , point-bifacial, point-partly-bifacial, point-unifacial, scraper-adze, scraper-continuous, scraper-end, scraper-lateral, scraper-NBK, scraper-thumbail, scraper-other, none	all
Raw Material	ceramic, CCS, glass, hornfels, igneous, ironstone, ochre, ostrich eggshell, pottery, quartz, quartzite, sandstone, silcrete, volcanic, indeterminate	all
Epoch	ESA, MSA, LSA, Khoi	all
Industry	Acheulean, Fauresmith, early MSA, Still Bay, Howiesons Poort, post-Howiesons Poort, late MSA, early LSA, Robberg Oakhurst, Wilton	all lithic
Broken?	yes, no	implements only
Maximum Dimension	continuous (measurement)	all
Longest Dimension Orthogonal to Maximum	continuous (measurement)	all
Longest Dimension Normal to Plane of Maximum and Second	continuous (measurement)	all

SOM TABLE 1. ALL ARTIFACT ATTRIBUTES RECORDED DURING PHASE I (continued).

Attribute	States	Applied to
Cortex Coverage	none, 1–25%, 26–50%, 51–75%, 76–100%	all lithic
Cortex Type	fluvial, outcrop, indeterminate, na	all lithic
Decoration	yes, no	all
Number of Notches	continuous (count)	implements only
Core Type	bipolar, discoidal, Levallois-Nubian, Levallois-preferential, Levallois-recurrent, minimal, opposed, other, other-prepared, rotated, single platform	cores only
Platform Preparation	yes, no	all lithic
Platform Faceting	yes, no	all lithic
Number of Blade Removals	continuous (count)	cores only
Number of Point Removals	continuous (count)	cores only
Largest Scar Length	continuous (measurement)	cores only
Single Plane of Initiations	yes, no	cores only
Scar Orientations to Single Plane	inclined, inclined-parallel, normal, Parallel, parallel-normal, na	cores only
Flaked Circumference of Plane in 45° Increments	continuous (count)	cores only
Primary Flaking Axis	intermediate, long, short, na	cores only
Primary Flaking Face	intermediate, long, short, na	cores only
Unifacial or Bifacial	yes, no	cores only
Equal Volume Either Side of Plane	yes, no, unclear	cores only
Similar Scar Sizes/Shapes Above and Below Plane	yes, no, unclear	cores only
Flaking Pattern on Primary Working Face	opposed, orthogonal, polydirectional, radial, subradial, unidirectional	cores only
Flaking Pattern on Secondary Working Face	opposed, orthogonal, polydirectional, radial, subradial, unidirectional	cores only
Coherent Flaking on Either Side of Plane (Initiations Align)	yes, no, unclear	cores only
Preferential Flake Removals	yes, no, unclear	cores only
Discolored	yes, no	all lithic
Decayed	yes, no	all lithic
Patinated	yes, no	all lithic
Double Patinated	yes, no	all lithic
Rounded Piece	yes, no	all lithic
Edge Rounding	yes, no	all lithic
Edge Damage (fracture)	yes, no	all lithic
Potlids	yes, no	all lithic
Grinding	yes, no	all lithic
Pitting	yes, no	all lithic
Additional Comments	free text	all
Photo Numbers	ID autopopulated	all

SOM TABLE 2. DESCRIPTION OF TIME-SENSITIVE ARTIFACTS.

Culture-Historic Period	Regional Dates	Time-Sensitive Artifact(s)	Artifact Descriptions	References
Acheulean	~1 Ma	handaxe	artifact that has been flaked on both faces (bifacially flaked)	Braun et al. 2013
Fauresmith	~350–450 ka	handaxe	similar to Acheulean handaxes, but on a smaller scale	Chazan et al. 2008; Potrat et al. 2010
early Middle Stone Age (eMSA)	>76 ka	denticulates?	large blades with retouch - denticulates	
Still Bay (SB)	70–77 ka	bifacial points	artifacts flaked bifacially (both surfaces)	Högberg and Larsson 2011
		blade cores?	prepared blade-like cores	
Howiesons Poort (HP)	60–65 ka	backed artifacts (segments)	blade blanks with steep retouch on one lateral margin, often shaped to a segment	Mackay 2011
		complex notch	multiple smaller removals in larger retouched removal	
		flat Levallois blade cores	flat Levallois cores with emphasis on blade production	
post-Howiesons Poort (pHP)	55 ka	Nubian-like	Levallois cores with an emphasis on distal preparation	Will, Mackay et al. 2014
		unifacial points	unifacially retouched flakes; although found throughout out the MSA, more common during the post-Howiesons Poort	
late Middle Stone Age	35 ka	flat prepared cores	short reduction sequence with minimal platform preparation; products will retain a large proportion of cortex on dorsal surface	Mackay et al. 2014
early Later Stone Age (eLSA)	23 ka	blade core	blade core with removals focused along narrow margin of core; sometimes one large platform preparation	Low, Mackay et al. 2017; Wadley 1993
Robberg	18 ka	bladelet core	bladelet cores on finer-grained material (CCS) that are often rotated to maximize reduction sequence	Beaumont 1978; Low and Mackay 2016; Porraz et al. 2016
Oakhurst	16 ka	Naturally Backed Knives (NBK)	naturally backed knives retain outcrop cortex on thicker lateral with scraper retouch on opposed lateral; usually characterized by a bedding plane dorsal surface and a flat (diffuse bulb) ventral surface	Deacon 1984; Sampson 1974
		pièce esquille	elongated scaled pieces (crushing on four margins) found in association with NBKs and anvils	
Wilton	6 ka	thumbnail scrapers	tiny steep scrapers on fine-grained material such as CCS	Deacon 1972, 1984; Wadley 2000
?		duck-billed scrapers	elongated scrapers with concave lateral margins and a splayed retouched distal on CCS	

URANIUM THORIUM DATING

Closed-system uranium-series dating of carbonate samples from Doring River localities UPK9 and UPK1 was undertaken by laser ablation multi-collector ICP-MS at the Wollongong Isotope Geochronology Laboratory, University of Wollongong. Laser ablation was performed with a New Wave Research 193 nm ArF excimer laser, equipped with a TV2 cell. Thorium (^{230}Th , ^{232}Th) and uranium (^{234}U , ^{235}U , ^{238}U) isotopes were measured on a Thermo Neptune Plus multi-collector ICP-MS mounted with jet sample and x-skimmer cones. All five isotopes were collected in static mode, with ^{230}Th and ^{234}U collected in ion counters. Helium flow rate and ICP-MS parameters were tuned with NIST612 element standard to derive a $^{232}\text{Th}/^{238}\text{U}$ ratio for this standard greater than 0.8 and thus minimize differences in fractionation between Th and U (Eggins et al. 1998). For tuning, a fluence of 2.35 J/cm², pulse rate of 5 Hz, spot size of 65 μm and scan speed of 5 μm/s was used. This yielded 0.8 V of ^{238}U and 0.7 V of ^{232}Th . Uranium-238 tail on ^{234}U , and ^{232}Th tail on ^{230}Th (although negligible for phosphates and carbonates) were measured using a coral and glass standard NIST612, respectively. Samples were ablated using rasters. Each raster was ~310 μm long and two passes were done on each raster. A fluence of 6.7 J/cm², pulse rate of 20 Hz, spot size of 150 μm and scan speed of 5 μm/s was used. Helium was used as a carrier gas at a flow rate of 0.9 L/min. Each raster was pre-ablated with a fluence of 2.9 J/cm², pulse rate of 5 Hz, spot size of 150 μm and scan speed of 200 μm/s. Before and after each sample, three rasters were done on NIST612, MK10 (a MIS 7 coral used as primary standard; [Woodroffe et al. 1991]), and MK16 (a MIS 5 coral used as secondary standard]). Measured $^{234}\text{U}/^{238}\text{U}$ and $^{230}\text{Th}/^{238}\text{U}$ isotopic ratios were corrected for elemental fractionation and Faraday cup/SEM yield by comparison with MK10 coral (see above) for which ratios were previously characterized internally by solution analysis. Concentrations of U and Th were determined using NIST612 glass as calibration standard. Background subtraction, concentration quantification, and ratio corrections were performed using Iolite™ software. The corrected ($^{234}\text{U}/^{238}\text{U}$) and ($^{230}\text{Th}/^{238}\text{U}$) activity ratios for the secondary standard (MK16 coral; 1.105±0.013 and 0.767±0.019, respectively; 2σ, n=11) were within error of the values determined by solution analysis (1.110±0.002 and 0.764±0.007) (parentheses denote activity ratios). The calculated closed-system ^{230}Th -U age for MK16 was calculated using IsoPlotR (Vermeesch 2018), using a detrital correction assuming a ($^{230}\text{Th}/^{232}\text{Th}$) of 0.8±0.8 for the detrital component. This returned an age of 120.87±1.07 ka (2σ, n=11), within error of the value determined by solution analysis (124±2 ka).

Ten rasters were produced on each of three samples taken from the immediate subsurface at UPK9 (S91090 and S91091; SOM Figure 1) and UPK1 (S910414). All samples show a large amount of detrital Th with ($^{232}\text{Th}/^{238}\text{U}$) activity ratios ranging from 0.27 to 0.36. For each sample, analyses were used to calculate an isochron age using IsoPlotR (Vermeesch 2018). A ($^{230}\text{Th}/^{238}\text{U}$) vs. ($^{232}\text{Th}/^{238}\text{U}$) isochron type and the maximum likelihood model were used. Decay

constants used for ^{230}Th and ^{234}U were 0.0091705±0.0000016 and 0.00282206±0.0000008 kyr⁻¹, respectively (Vermeesch 2018). Calculated isochron ages for S91090 and S91091 are respectively 226±25 ka (2σ, n=10; SOM Figure 2) and 202±48 ka (2σ, n=10; SOM Figure 3). Note, however, that there is only a small spread on ($^{232}\text{Th}/^{238}\text{U}$) values for S91091 (see SOM Figure 3), such that the robustness of the calculated age for this sample is poor. Sample S910414 did not return any meaningful isochron (SOM Figure 4).

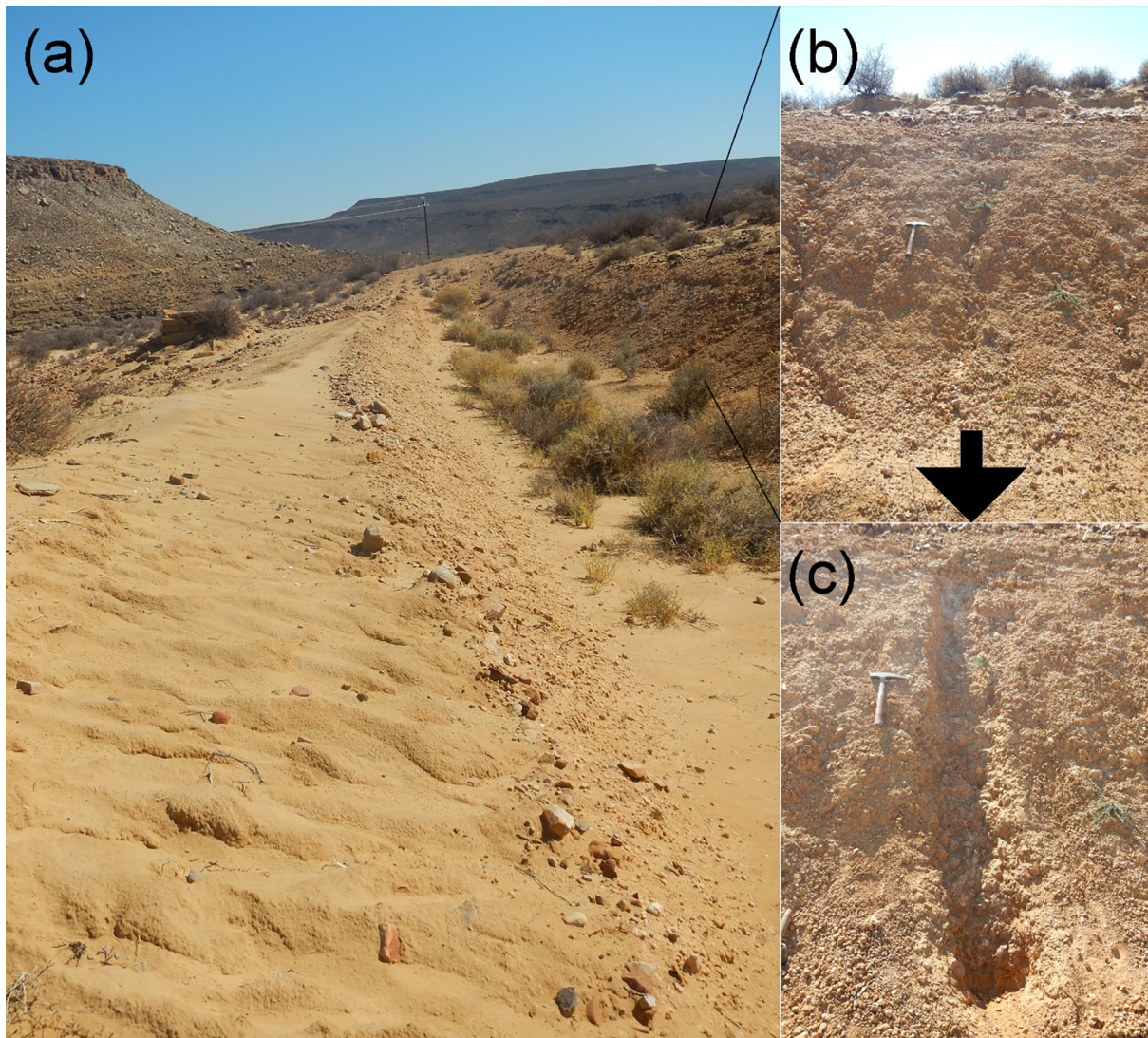
OPTICALLY STIMULATED LUMINESCENCE (OSL) DATING

Three sediment samples were collected for OSL dating, which were processed at the Luminescence Geochronology Lab at the University of Nebraska, Lincoln, USA.

Sample preparation was carried out under amber-light conditions. Samples were wet sieved to extract the 90–150 μm fraction, and then treated with HCl to remove carbonates and with hydrogen peroxide to remove organics. Quartz and feldspar grains were extracted by flotation using a 2.7 gm cm⁻³ sodium polytungstate solution, then treated for 75 minutes in 48% HF, followed by 30 minutes in 47% HCl. The sample was then resieved and the <90 μm fraction discarded to remove residual feldspar grains. The etched quartz grains were mounted on the innermost 2 mm or 5 mm of 1 cm aluminium disks using Silkospray.

Chemical analyses were carried out using a high-resolution gamma spectrometer. Dose-rates were calculated using the method of Adamiec and Aitken (1998) and Aitken (1998). The cosmic contribution to the dose-rate was determined using the techniques of Prescott and Hutton (1994).

Optically stimulated luminescence analyses were carried out on Risø Automated OSL Dating System Models TL/OSL-DA-15B/C and TL/OSL-DA-20, equipped with blue and infrared diodes, using the Single Aliquot Regenerative Dose (SAR) technique (Murray and Wintle 2000). Early background subtraction was used (Ballarini et al. 2007, Cunningham and Wallinga 2010). Prior to optical stimulation, sample UNL3808 was preheated to 200°C for 10s with a cutheat of 180°C for 0s, and samples UNL3809 and UNL3810 were preheated to 240°C for 10s with a cutheat of 220°C for 0s. These temperatures were based upon preheat plateau tests between 180°C and 280°C. Dose-recovery and thermal transfer tests were also conducted (Murray and Wintle 2003). Preheat plateau, dose recovery, and thermal transfer test results for UNL3808 are provided in SOM Table 3, and SOM Figures 5 and 6. Growth curves were examined to determine whether the samples were below saturation ($D/D_0 < 2$; (Wintle and Murray 2006)). Optical ages are based upon a minimum of 50 aliquots (Rodnight 2008). Individual aliquots were monitored for insufficient count-rate, poor quality fits (i.e., large error in the equivalent dose, D_0), poor recycling ratio, strong medium vs. fast component (Durcan and Duller 2011), and detectable feldspar. Aliquots deemed unacceptable based upon these criteria were discarded from the data set prior to averaging. Calculation of sample D_0 values was carried out using the Central Age Model (CAM) (Galbraith et al. 1999) unless



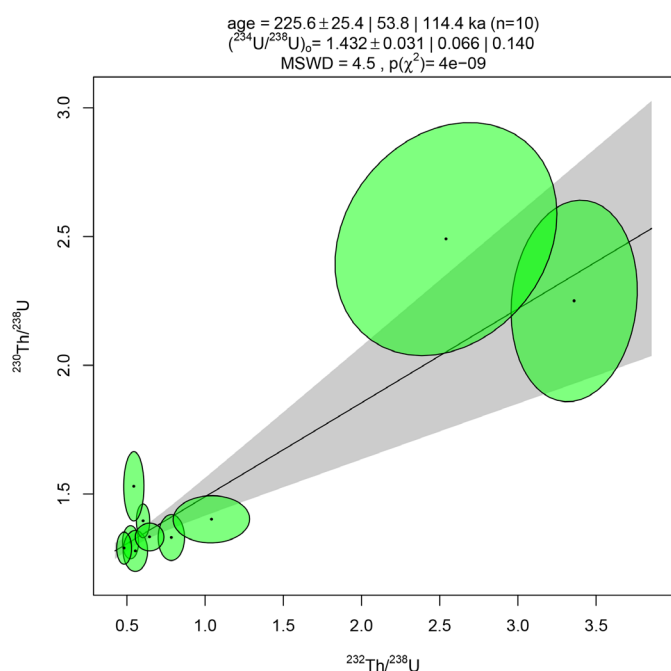
SOM Figure 1. Location from which samples S91090 and S91091 were taken at UPK9. (a) Old cutting at UPK1, probably excavated to constrain runoff from the nearby road. (b) North face of the cutting. (c) Trench from which samples S91090 and S91091 were taken.

the D_e distribution (asymmetric distribution; decision table of Bailey and Arnold [2006]), indicated that the Minimum Age Model (MAM) (Galbraith et al. 1999) was more appropriate.

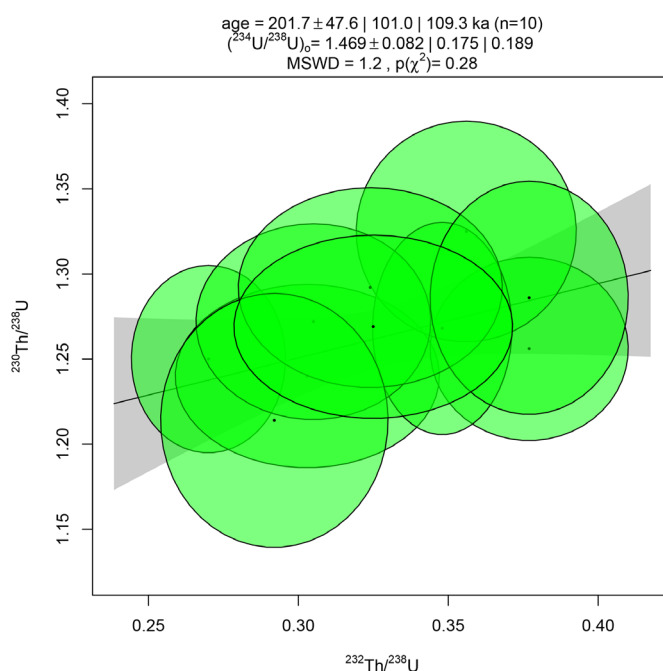
Dose rates, D_e values, and OSL ages for all three samples are provided in SOM Table 4.

REFERENCES

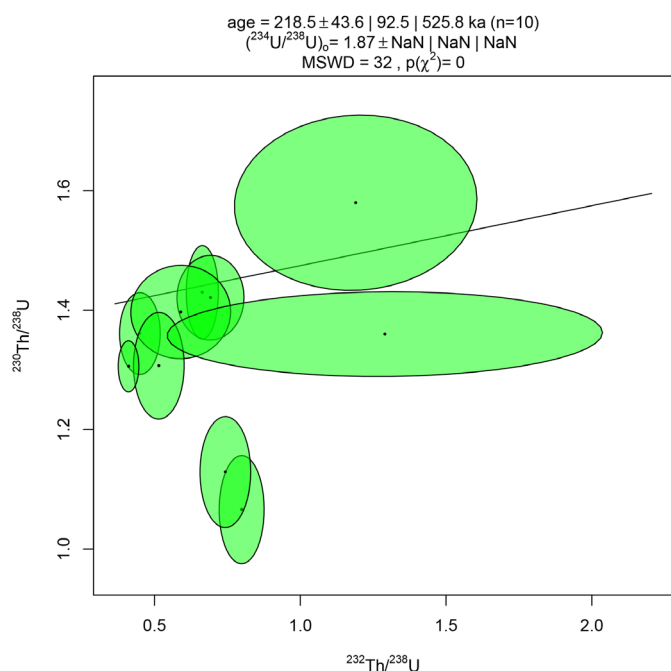
- Adamiec, G. and M. Aitken. 1998. Dose-rate conversion factors: update. *Ancient TL* 16: 37–50.
- Aitken, M.J. 1998. *An Introduction to Optical Dating*. Oxford, Oxford University Press.
- Bailey, R.M. and L.J. Arnold. 2006. Statistical modelling of single grain quartz D_e distributions and an assessment of procedures for estimating burial dose. *Quaternary Science Reviews* 25(19–20): 2475–2502.
- Ballarini, M., J. Wallinga, A.G. Wintle, and A.J.J. Bos. 2007. A modified SAR protocol for optical dating of individual grains from young quartz samples. *Radiation Measurements* 42(3): 360–369.
- Beaumont, P.B. 1978. *Border Cave*. M.A. thesis, Cape Town, University of Cape Town.
- Braun, D.R., N.E. Levin, D. Styrder, A.I.R. Herries, W. Archer, F. Forrest, D.L. Roberts, L.C. Bishop, T. Matthews, S.B. Lehmann, R. Pickering, and K.E. Fitzimmons. 2013. Mid-Pleistocene hominin occupation at Elandsfontein, Western Cape, South Africa. *Quaternary Science Reviews* 82: 145–166.
- Chazan, M., H. Ron, A. Matmon, N. Porat, P. Goldberg, R. Yates, M. Avery, A. Sumner, and L.K. Horowitz. 2008. Radiometric dating of the Earlier Stone Age sequence in Excavation 1 at Wonderwerk Cave, South Africa: preliminary results. *Journal of Human Evolution* 55: 1–11.
- Cunningham, A.C. and J. Wallinga. 2010. Selection of integration time intervals for quartz OSL decay curves. *Quaternary Geochronology* 5(6): 657–666.
- Deacon, J. 1972. Wilton: an assessment after fifty years. *South African Archaeological Bulletin* 27: 10–48.



SOM Figure 2. Isochron diagram for sample S91090, produced using IsoPlotR (Vermeesch 2018). The x and y axes represent ($^{232}\text{Th}/^{238}\text{U}$) and ($^{230}\text{Th}/^{238}\text{U}$) activity ratios, respectively. Each analysis is shown with its ellipsoid of error. The black line represents the calculated isochron and the grey area the 2σ confidence interval on the isochron.



SOM Figure 3. Isochron diagram for sample S91091, produced using IsoPlotR (Vermeesch 2018). The x and y axes represent ($^{232}\text{Th}/^{238}\text{U}$) and ($^{230}\text{Th}/^{238}\text{U}$) activity ratios, respectively. Each analysis is shown with its ellipsoid of error. The black line represents the calculated isochron and the grey area the 2σ confidence interval on the isochron.

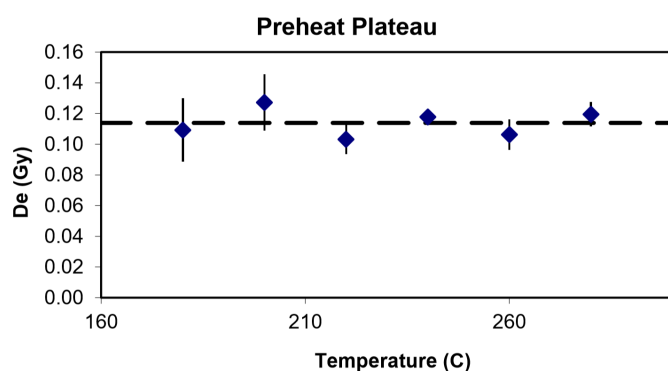


SOM Figure 4. Isochron diagram for sample S910414, produced using IsoPlotR (Vermeesch 2018). The x and y axes represent ($^{232}\text{Th}/^{238}\text{U}$) and ($^{230}\text{Th}/^{238}\text{U}$) activity ratios, respectively. Each analysis is shown with its ellipsoid of error. The black line represents the calculated isochron and the grey area the 2σ confidence interval on the isochron. Because of the spread in the data and the poor resulting isochron, the calculated age for this sample was not retained.

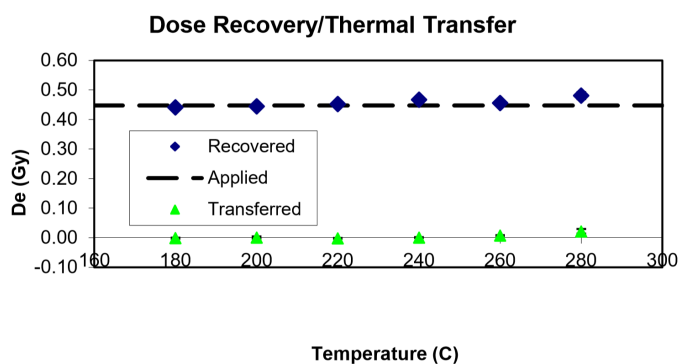
- Deacon, J. 1984. *The Later Stone Age of Southernmost Africa*. Oxford, British Archaeological Reports International Series 213.
- Durcan, J.A. and G.A.T. Duller. 2011. The fast ratio: a rapid measure for testing the dominance of the fast component in the initial OSL signal from quartz. *Radiation Measurements* 46(10): 1065–1072.
- Eggins, S., L.P.J. Kinsley and J.M.G. Shelley. 1998. Deposition and element fractionation processes during atmospheric pressure laser sampling for analysis by ICP-MS. *Applied Surface Science* 127-129: 278–286.
- Galbraith, R., R.G. Roberts, G.M. Laslett, H. Yoshida, and J.M. Olley. 1999. Optical dating of single and multiple grains of quartz from Jimnium Rock Shelter, Northern Australia: Part I, experimental design and statistical models. *Archaeometry* 41: 339–364.
- Högberg, A. and L. Larsson. 2011. Lithic technology and behavioural modernity: new results from the Still Bay site, Hollow Rock Shelter, Western Cape Province, South Africa. *Journal of Human Evolution* 61: 133–155.
- Low, M., A. Mackay, and N. Phillips. 2017. Understanding the Earl Later Stone Age technology at a landscape-scale: evidence from the open-air locality Uitspankraal (UPK7) in the Western Cape, South Africa. *Azania: Archaeological Research in Africa*, 52(3): 373–406.
- Low, M. and A. Mackay. 2016. The late Pleistocene microlithic at Putslaagte 8 rockshelter in the Western Cape, South Africa. *South African Archaeological Bulletin* 71(204): 146–159.

SOM TABLE 3. PREHEAT PLATEAU, DOSE RECOVERY, AND THERMAL TRANSFER TEST RESULTS FOR UNL3808.

Preheat Temperature (°C)	De (Gy)		
	Preheat Plateau	Dose Recovery Test*	Thermal Transfer Test
180	0.11±0.02	0.44±0.01	0.00±0.00
200	0.13±0.02	0.44±0.00	0.00±0.00
220	0.10±0.01	0.45±0.00	0.00±0.00
240	0.12±0.00	0.47±0.00	0.00±0.00
260	0.11±0.01	0.46±0.01	0.01±0.00
280	0.12±0.01	0.48±0.01	0.02±0.01



SOM Figure 5. Preheat plateau test results for UNL3808.



SOM Figure 6. Dose recovery and thermal transfer test results for UNL3808.

Mackay, A. 2011. Nature and significance of the Howiesons Poort to post-Howiesons Poort transition at Klein Kliphuis rock shelter, South Africa. *Journal of Archaeological Science* 38: 1430–1440.

Mackay, A., A. Sumner, Z. Jacobs, B. Marwick, K. Bluff, and M. Shaw. 2014. Putslaagte 1 (PL1), the Doring River, and the later Middle Stone Age in southern Africa's Winter Rainfall Zone. *Quaternary International* 350 1–16.

Murray, A.S. and A.G. Wintle. 2003. The single aliquot regenerative dose protocol: potential for improvements in reliability. *Radiation Measurements* 37(4–5): 377–381.

Porat, N., M. Chazan, R. Grün, M. Aubert, V. Eisenmann, and L.K. Horowitz. 2010. New radiometric ages for the Fauresmith industry from Kathu Pan, southern Africa: implications for the Earlier and Middle Stone Age transition. *Journal of Archaeological Science* 37: 269–283.

Porraz, G., M. Igrreja, P. Schmidt, and J.E. Parkington. 2016. A shape to the microlithic Robberg from Elands Bay Cave (South Africa). *Southern African Humanities* 29: 203–247.

Prescott, J.R. and J.T. Hutton. 1994. Cosmic ray contributions to dose rates for luminescence and ESR dating:

SOM TABLE 4. RESULTS OF MULTIPLE-ALIQUOT OSL DATING OF NEAR-SURFACE SEDIMENTS FROM UPK7.*

UNL#	Burial Depth (m)	H ₂ O (%)	K ₂ O (%)	±	U (ppm)	±	Th (ppm)	±	Cosmic (Gy)	Dose Rate (Gy/ka)	Age Model	D _e (Gy)	N Aliquots	Age (ka)
UNL-3808	0.3	0.78	0.85	0.05	1.69	0.13	5.55	0.37	0.19	1.70±0.07	CAM	0.13±0.01	66	0.077±0.005
											MAM	0.116±0.006		0.069±0.005
UNL-3809	0.7	1.91	1.15	0.05	1.76	0.13	7.31	0.39	0.19	2.05±0.08	CAM	62.28±0.67	52	30.3±1.3
UNL-3810	0.5	6.72	1.00	0.05	1.61	0.13	5.86	0.37	0.19	1.71±0.07	CAM	52.01±0.63	60	30.5±1.4

*Moisture content was measured *in situ*. Error on D_e is at 1 standard error. Error on age includes random and systematic errors calculated in quadrature.

- large depths and long-term time variations. *Radiation Measurements* 23: 497–500.
- Rodnight, H. 2008. How many equivalent dose values are needed to obtain a reproducible distribution? *Ancient TL* 26: 3–9.
- Sampson, C.G. 1974. *The Stone Age Archaeology of Southern Africa*. New York, Academic Press.
- Soriano, S., P. Villa, and L. Wadley. 2007. Blade technology and tool forms in the Middle Stone Age of South Africa: the Howiesons Poort and post-Howiesons Poort at Rose Cottage Cave. *Journal of Archaeological Science* 34: 681–703.
- Vermeesch, P. 2018. IsoplotR: a free and open toolbox for geochronology. *Geoscience Frontiers* 9(5): 1479–1493.
- Wadley, L. 1993. The Pleistocene Later Stone Age south of the Limpopo River. *Journal of World Prehistory* 7 (3): 243–296.
- Wadley, L. 2000. The Wilton and Pre-Ceramic Post-Classic Wilton Industries at Rose Cottage Cave and their context in the South African sequence. *The South African Archaeological Bulletin* 55 (172): 90–106.
- Will, M., A. Mackay, and N. Phillips. 2015. Implications of Nubian-like core reduction systems in southern Africa for the identification of early modern human dispersals. *PLoS One* 10(6): e0131824.
- Wintle, A.G. and A.S. Murray. 2006. A review of quartz optically stimulated luminescence characteristics and their relevance in single-aliquot regeneration dating protocols. *Radiation Measurements* 41(4): 369–391.
- Woodroffe, C.D., S.A. Short, D.R. Stoddart, T. Spencer, and R.S. Harmon. 1991. Stratigraphy and chronology of late Pleistocene reefs in the Southern Cook Islands, South Pacific. *Quaternary Research* 35: 246–263.